Caulobacter crescentus adapts to phosphate-starvation by synthesizing anionic glycoglycerolipids and a novel glycosphingolipid

Gabriele Stankeviciute[a], Ziqiang Guan[b], Howard Goldfine[c], Eric A. Klein [a, d, #]

[a] Center for Computational and Integrative Biology, Rutgers University-Camden, Camden, New Jersey, USA

[b] Department of Biochemistry, Duke University Medical Center, Durham, North Carolina, USA

[c] Department of Microbiology, University of Pennsylvania, Philadelphia, Pennsylvania, USA

[d] Department of Biology, Rutgers University-Camden, Camden, New Jersey, USA

Running Head: *C. crescentus* produces anionic glycolipids

[#] Address correspondence to Eric A. Klein, eric.a.klein@rutgers.edu

Abstract word count: 212

Text word count: 4,138

Abstract: *Caulobacter crescentus* adapts to phosphate starvation by elongating its cell body and a polar stalk structure. The stalk is an extension of the Gram-negative envelope containing inner- and outer-membranes as well as a peptidoglycan cell wall. Cellular elongation requires a 6-7 fold increase in membrane synthesis, yet phosphate limitation would preclude the incorporation of additional phospholipids. In the place of phospholipids, *C. crescentus* can synthesize several glycolipid species including a novel glycosphingolipid (GSL-2). While glycosphingolipids are ubiquitous in eukaryotes, the presence of GSL-2 in *C. crescentus* is surprising since GSLs had only previously been found in *Sphingomonas* species where they play a role in outer-membrane integrity. In this paper, we identify three proteins required for GSL-2 synthesis: CcbF catalyzes the first step in ceramide synthesis while Sgt1 and Sgt2 sequentially glycosylate ceramides to produce GSL-2. Unlike in *Sphingomonas*, GSLs are non-essential in *C. crescentus*; however, the presence of ceramides does contribute to phage resistance and susceptibility to the cationic antimicrobial peptides polymyxin B. The identification of a novel lipid species specifically produced upon phosphate starvation suggests that bacteria may be able to synthesize a wider variety of lipids in response to stresses than previously observed. Uncovering these lipids and their functional relevance will provide greater insight into microbial physiology and environmental adaptation.

Importance: Bacteria adapt to environmental changes in a variety of ways including altering their cell shape. *Caulobacter crescentus* adapts to phosphate starvation by elongating its cell body and a polar stalk structure containing both inner- and outer-membranes. While we generally think of cellular membranes being composed largely of phospholipids, cellular elongation occurs when environmental phosphate, and therefore phospholipid synthesis, is limited. In order to

adapt to these environmental constraints, *C. crescentus* synthesizes several glycolipid species including a novel glycosphingolipid. This finding is significant because glycosphingolipids, while ubiquitous in eukaryotes, are extremely rare in bacteria. In this paper, we identify three proteins required for GSL-2 synthesis and demonstrate that they contribute to phage resistance. These findings suggest that bacteria may synthesize a wider variety of lipids in response to stresses than previously observed.

Introduction

Regulation of cell membrane composition is critical for an organism's ability to adapt to environmental perturbations. In poikilothermic species, cells must alter their cell membrane in response to temperature changes in order to maintain relatively constant membrane fluidity. For bacteria such as *Escherichia coli*, cells incorporate an increasing proportion of unsaturated fatty acids as temperatures decrease (1, 2); the kinks introduced by acyl chain unsaturation decrease membrane viscosity to counteract the effects of lower temperature. Similarly, a variety of Gram-positive and Gram-negative bacteria alter the ratio of phospholipid headgroups in response to osmotic shock (3); *E. coli* increases the ratio of cardiolipin:phosphatidylethanolamine when osmotically stressed (4).

Oligotrophic bacteria require adaptations to stresses associated with nutrient availability. For example, nutrient levels in fresh-water lakes experience seasonal fluctuations and phosphate concentration has been shown to be a limiting factor for bacterial growth (5). The oligotrophic Gram-negative bacterium *Caulobacter crescentus* responds to phosphate limitation by dramatically elongating its cell body and a polar stalk structure, a thin extension of the cell envelope, consisting of an inner membrane, peptidoglycan cell wall, an outer-membrane, and a surface-layer (6) (Fig. 1A). The stalk has been hypothesized to serve as means to increase phosphate uptake (7) since all four members of the PstSCAB high-affinity phosphate import pathway are found in the stalk (7, 8). Additionally, analytical modeling of nutrient diffusion suggests that stalk elongation is the most efficient method of increasing nutrient flux to the cell while minimizing cell surface area and volume (8). Under phosphate-rich growth conditions, cells are approximately 1 μm in length, stalks are very short (~100 nm), and phosphatidylglycerol accounts for approximately 30% of total lipids (9). Upon phosphate

starvation, cell bodies and stalks can grow up to 3.5 μm and 15 μm in length, respectively, which requires significant production of new lipids to build the inner and outer membranes. When phosphate is limited it is unlikely that this new membrane contains phospholipids, therefore we hypothesized that *C. crescentus* synthesizes alternative lipids for cellular and stalk elongation.

Several Alphaproteobacteria adapt to phosphate limitation by increasing the production of glyceroglycolipids and ornithine lipids. For example, *Agrobacterium tumefaciens* synthesizes monoglucosyl diacylglycerol (DAG), glucuronosyl diacylglycerol, and diacylglycerol trimethylhomoserine (DGTS) (10, 11) while *Mesorhizobium loti* produces di- and triglycosyldiacylglycerols, DGTS, and ornithine lipid (12). Glycolipids make up a large proportion of the *C. crescentus* membrane even in phosphate-rich growth media (45%-62%) (9), but phosphate-mediated changes in lipid composition have not been characterized. We hypothesized that during phosphate-limitation *C. crescentus* either 1) increases the proportion of existing glycolipids or 2) synthesizes novel lipid species to replace phospholipids.

Analysis of total membrane composition following phosphate-limitation revealed that both hypotheses were correct. *C. crescentus* increases the amount of monohexuronosyl DAG (MHDAG) and synthesizes a novel hexosyl-hexuronosyl-ceramide glycosphingolipid (HexHexA-Cer). This glycosphingolipid (GSL) represents a novel bacterial lipid species. In this report we characterize this GSL, identify the enzymes responsible for initiating ceramide synthesis and its sequential glycosylation, and address the physiological importance of ceramide-based lipids.

Results

Phosphate limitation induces changes in membrane composition

Phosphate starvation induces elongation of both the cell body and stalk in *C. crescentus* (Fig. 1A). If we approximate the shapes of the cell body and stalk as cylinders, we can estimate that the total surface area of the cell, and thus the synthesis of membrane lipids, increases 6 to 7-fold upon phosphate limitation. This significant increase in membrane area suggests that *C. crescentus* must be able to produce alternatives to phospholipids during phosphate starvation. Indeed, when we compare the total lipid composition under phosphate-rich (1 mM phosphate) and phosphate-starved (1 μM phosphate) conditions by using normal phase liquid chromatography/tandem mass spectrometry (LC/MS/MS), we see a dramatic decrease in phosphatidylglycerol and a corresponding increase in several species of glycolipids (Fig. 1B). In particular, phosphate starvation induces the synthesis of mono- and di-glycosyl diacylglycerols as well as a GSL, hexose-hexuronic acid-ceramide (HexHexA-Cer; C16 ceramide (d18:1/16:0)) (Fig. 1B). These lipid species were identified by exact mass measurement in conjunction with collision-induced dissociation (CID) tandem mass spectrometry. The presence of a GSL was unexpected since sphingolipids, while highly abundant in eukaryotes, are rarely found in bacteria. Some species in the *Bacteroides*, *Porphyromonas*, and *Prevotella* genera are capable of synthesizing the phosphosphingolipids ceramide phosphorylethanolamine and/or ceramide phosphoglycerol (13). Non-phosphate containing GSLs, have only been described in the family Sphingomonadaceae where they can function as a substitute for lipopolysaccharide (LPS) (14). Structural analyses of *Sphingomonas* GSLs have revealed carbohydrate moieties containing 1, 3, or 4 sugar units (Fig. 1C) (14, 15). By contrast, the GSL found in *C. crescentus* has two sugars and thus represents a novel bacterial GSL species we named GSL-2 (Fig. 1C).

Ceramide synthesis in C. crescentus

Sphingolipid synthesis begins with the production of a ceramide molecule which is then modified with various polar groups. In eukaryotes, ceramide synthesis is a four-step process that begins with the condensation of serine and a fatty acyl-CoA to produce 3-oxo-sphinganine in a reaction catalyzed by oxoamine synthase (16). While each of the enzymatic steps in ceramide synthesis have been well characterized in eukaryotes (17), only the oxoamine synthase enzyme required for the first step appears to be conserved in bacteria. Indeed, bacterial species have been identified encoding one or more oxoamine synthases including: serine palmitoyltransferase (Spt), 8-amino-7-oxononanoate synthase (BioF), 5-aminolevulinate synthase (HemA), and 2-amino-3-oxobutyrate coenzyme A ligase (Kbl) (18). *C. crescentus* encodes three putative oxoamine synthases: CCNA_01220 (BioF), CCNA_01417 (HemA), and CCNA_01647 (BioF).

To assess the role of the candidate oxoamine synthases in ceramide synthesis, total lipid composition was analyzed in wild-type, Δ*ccna_01220*, and *Δccna_01647* cells. We were unable to obtain a deletion of *ccna_01417* since this is an essential gene (19); however, recent biochemical analysis of CCNA_01417 reveals that it is most likely involved in the production and regulation of heme co-factors (20). Ceramides were completely absent in the Δ*ccna_01220* strain (Fig. 2), therefore we will refer to this gene as *Caulobacter crescentus* BioF (*ccbF*). Complementation of the *ccbF* deletion restored ceramide synthesis (Fig. S1A). Interestingly, deletion of BioF homolog CCNA_01647 had no effect on ceramide synthesis despite having 51% similarity and 35% identity to CcbF (Fig. 2). We note that while the *ccna_01647* deletion did not affect ceramide levels, we observed a reduction in MHDAG synthesis (Fig. 2), though the mechanism for this decrease is unknown.

Glycosphingolipid synthesis requires two sequential glycosyltransferases

GSL-2 has a novel glycosylation pattern consisting of a hexose and a hexuronic acid (Fig. 1C). Lipid glycosylation, in both eukaryotes and prokaryotes, is performed by GT-4 family glycosyltransferases; *C. crescentus* encodes 11 putative GT-4 glycosyltransferases (21). To identify the glycosyltransferases required for GSL-2 synthesis we narrowed down the list of candidate genes using the following criteria: 1) genes upregulated upon phosphate starvation (22), 2) non-essential genes (19), and 3) genes without a direct homolog in *E. coli*, since *E. coli* does not produce GSLs. Of the 11 initial candidates, only two genes fit all three criteria: *ccna_00792* and *ccna_00793* (Fig. 3A and Table S4). Both candidate genes are part of the PhoB regulon which contains genes upregulated under phosphate starvation conditions (Fig. 3B) (22). Deletion of *ccna_00792* or *ccna_00793* results in a complete lack of diglycosylated ceramide (Fig. 3C) whereas deleting *ccna_00792* leads to the accumulation of the monoglycosylated HexA-Cer species (Fig. 3D). Complementation of these deletions recovered ceramide glycosylation (Fig. S1B-C). These data support a model of sequential ceramide glycosylation by CCNA_00793 and CCNA_00792, which we are naming Sphingolipid Glycosyltransferase 1/2 (Sgt1/2), respectively (Fig. 3E). Sgt1 functions as a glucuronosyltransferase, adding a hexuronic acid, while Sgt2 is a glycosyltransferase responsible for adding a hexose sugar. Sgt1/2 appear to specifically glycosylate sphingolipids as neither deletion affected the glycosylation of DAG-based lipids (Fig. 3C-D). The specificity of Sgt1/2 was further confirmed by heterologous expression in *E. coli* where we could only detect non-glycosylated lipids (Fig. S2A-B).

While GSL-2 synthesis occurs in response to phosphate starvation, neither ceramides nor GSL-2 appear to be necessary for stalk biogenesis or cell elongation (Fig. S3A). This is likely

due to the sufficiency of upregulated DAG lipids in low-phosphate (Fig. 1B). Unlike GSL-2, non-glycosylated ceramides are produced across a wide range of phosphate concentrations, albeit at lower levels in the presence of excess phosphate (Fig. S3B). Surprisingly, *ccbF* mRNA levels are reduced during phosphate starvation, despite higher levels of ceramide production (Fig. S3C). Restriction of ceramide glycosylation to growth environments in which phospholipid synthesis is limited appears to be critical for membrane homeostasis. Overexpression of Sgt1 and Sgt2 in high-phosphate media results in the production of both HexA-Cer and GSL-2 (Fig. 4A-C). Unlike physiological glycosphingolipid production during phosphate starvation, Sgt1/2 overexpression leads to an accumulation of HexA-Cer (compare Fig 1B to 4A). Furthermore, we do not detect HexHexA-DAG under these conditions providing additional evidence that Sgt1/2 specifically glycosylates ceramide lipids (Fig. 4C). The production of glycosphingolipids in high-phosphate leads to cell lysis as assessed by propidium iodide staining (Fig. 4D). This phenomenon may be due to an excess of anionic lipids and is consistent with our previous observation that overabundance of anionic phospholipids is detrimental in *E. coli* (23).

Ceramides regulate antibiotic and phage susceptibility

Under laboratory growth conditions, ceramides and GSLs are nonessential; cell growth is minimally perturbed in *ccbF* and *sgt1* deletion strains whether grown in high- (1 mM) or low- (1 μM) phosphate minimal media (Fig. 5A-B). GSL-producing *Sphingomonas* species are resistant to the antibiotic polymyxin B (24); therefore, we tested whether ceramides or GSL-2 conferred similar resistance in *C. crescentus*. Surprisingly, the deletion of *ccbF* increased resistance to polymyxin B in both high and low phosphate (Fig. 5A-B). In low phosphate, the Δ*sgt1* strain did not have increased polymyxin B resistance demonstrating that the resistance phenotype was

specifically due to the presence of ceramide lipids regardless of their glycosylation (Fig. 5B) In both phosphate conditions, complementation of *ccbF* restored sensitivity to polymyxin B (Fig. 5A-B).

Modifying the bacterial envelope structure and composition can also affect cellular interactions with bacteriophages. Phage ΦCr30 infects *C. crescentus* by attaching to the extracellular surface-layer (S-layer) (25). Growth curves of wild-type and *ccbF* deletion strains infected with ΦCr30 in PYE demonstrated that ceramides are important for increasing phage resistance (Fig. 5C); this initial screen was performed in PYE because ΦCr30 infections are generally inhibited in minimal media (26). The increased susceptibility of the Δ*ccbF* strain could be attributed to either enhanced phage adsorption or an increased viral burst-size. We tested the ability of ΦCr30 to adsorb to wild-type, Δ*ccbF*, and Δ*sgt1* cells in HIGG- 1μM phosphate. Both of the mutant strains had an enhanced rate of phage adsorption which was restored to normal upon complementation (Fig. 5D), suggesting that mature GSL-2 is required to inhibit phage adsorption. Measurements of burst-size did not reveal any differences between the strains in low phosphate (Fig. 5E); however, the *ccbF* and *sgt1* deletion strains appear to have shorter latent periods consistent with faster phage adsorption to these cells (Fig. 5E).

Phage ΦCr30 attaches to *C. crescentus* by binding to the cell envelope S-layer, a crystalline lattice composed of the protein RsaA (27). The S-layer is, in turn, anchored to the cell through interactions with the O-antigen domain of lipopolysaccharide (LPS) (28). A comparison of LPS and S-layer production in wild type and GSL mutants did not reveal any remarkable distinctions between the strains (Fig. S4A-B), suggesting that the enhanced phage adsorption observed in the GSL mutants is not due to an increase in S-layer production. The accessibility of the S-layer to phage is restricted by the production of an exopolysaccharide (EPS) capsule (29).

To test whether the absence of ceramides disrupts EPS production, *C. crescentus* strains were grown in HIGG-1 μM phosphate and incubated with FITC-labeled dextran (29). The wide zone-of-exclusion around the wild-type and Δ*ccbF* cells show that they produce EPS, in contrast to the non-EPS producing ΔMGE strain (29) (Fig. S4C).

Discussion

C. crescentus adapts to phosphate limitation, in part, by dramatically elongating both its cell body and polar stalk appendage (7, 30) (Fig. 1A) requiring a significant amount of lipid synthesis. Without the environmental phosphate required for phospholipid synthesis, *C. crescentus* upregulates the production of several glycolipid species including a novel glycosphingolipid, GSL-2 (Fig. 1B). In this study, we identify three enzymes involved in GSL production: CcbF is responsible for the first step of ceramide synthesis (Fig. 2) while Sgt1 and Sgt2 sequentially glycosylate ceramide to yield GSL-2 (Fig. 3C-E).

Upregulation of glycolipid synthesis in response to phosphate limitation has been previously described for *Agrobacterium tumefaciens* and *Mesorhizobium loti* (11, 12). In these species, cells produce nonphosphorus glycosyl-DAGs. While *C. crescentus* also produces mono- and diglycosyl-DAGs, this is the first demonstration of bacterial GSL synthesis in response to phosphate starvation. While GSLs are found ubiquitously in eukaryotic organisms, their presence in bacteria was thought to be limited to species of the family Sphingomonadaceae. In *Sphingomonas* species, GSLs are used as a substitute for LPS in the outer membrane and contain 1, 3, or 4 sugar units (14, 15). *Sphingomonas wittichii* strain RW1 produces two different monoglycosylated GSLs in place of LPS (31). Not surprisingly, serine palmitoyltransferase, which catalyzes the first step of ceramide synthesis, is an essential gene in *S. wittichii* (32). By

234 contrast, *C. crescentus* GSL-synthesis genes are non-essential and GSL-2 is produced even in the
235 presence of LPS (Fig. S4A). Furthermore, ablation of ceramide or GSL-2 has no effect on
236 proliferation (Fig. 5A-B) or cellular elongation (Fig. S3A). Thus, we conclude that while GSL
237 production occurs under conditions of phosphate limitation, it is dispensable for cell elongation,
238 stalk synthesis, and survival. This is likely due to the presence of sufficient glycosylated-DAGs
239 to compensate for the loss of GSLs.

240 This study is the first to identify bacterial glycosyltransferase enzymes required for
241 ceramide glycosylation. As expected, BLAST homology searches (33) demonstrate that outside
242 of the Caulobacteraceae family, Sgt1 and Sgt2 are most homologous to glycosyltransferases in
243 the GSL-producing Sphingomonadaceae family. Unlike many other bacterial
244 glycosyltransferases which demonstrate a high degree of promiscuity regarding sugar acceptors
245 (34, 35), Sgt1 appears to have a high degree of specificity towards ceramide glycosylation.
246 Deletion of *sgt1* in *C. crescentus* has no effect on glycosyldiacylglycerol production (Fig. 3C)
247 and heterologous expression of Sgt1 and Sgt2 in *E. coli* does not lead to lipid glycosylation (Fig.
248 S2).

249 While *Sphingomonas* species use GSLs to replace LPS, the role of GSLs in *C. crescentus*
250 is less clear. Ceramide synthesis occurs over a wide range of phosphate concentrations, yet
251 mature GSLs are only produced during phosphate starvation. Complete deletion of ceramides
252 appears to alter the function of *C. crescentus* membranes resulting in increased resistance to the
253 lipid-interacting antibiotic polymyxin B and increased sensitivity to phage-mediated killing (Fig.
254 5A-C). These effects occur despite the absence of gross changes to LPS, S-layer, or EPS
255 production (Fig. S4A-C). Resistance to cationic antimicrobial peptides like polymyxin B often
256 occurs by reducing the negative charge of the membrane to prevent binding; for example, in *E.*

coli, lipid A is modified with 4-amino-4-deoxy-L-arabinose (36) to neutralize charge. In *C. crescentus*, the impact of ceramide or GSL deficiency on total membrane charge is less clear; non-glycosylated ceramides are neutral while the hexuronic acid found in GSL-2 is anionic. Therefore, the relative abundances of all lipid species would be required to assess the role of membrane charge in antibiotic resistance.

The increased susceptibility of ceramide-depleted cells to phage lysis appears to be due to enhanced phage adsorption to the *ccbF* and *sgt1* deletion strains (Fig. 5D). Increased adsorption reduces the phage latency period without affecting the phage burst-size (Fig. 5E). Although the abundance of S-layer protein is not affected in the GSL mutants (Fig. S4B), recent biophysical studies have shown that the S-layer protein RsaA can exist on the cell surface in either a crystalline or aggregated state (37). This is consistent with cryo-electron tomography showing distinct regions of S-layer organization in intact *C. crescentus* cells (38). While we do not know exactly how phage Cr30 binds to the S-layer, it is possible that GSLs affect S-layer organization, rather than production, thereby regulating phage interactions.

Materials and Methods

Bacterial strains, plasmids, and growth conditions

The strains, plasmids, and primers used in this study are described in Supplemental Tables S1, S2, and S3, respectively. Details regarding strain construction are available in the Supplementary Methods. *C. crescentus* wild-type strain NA1000 and its derivatives were grown at 30 °C in peptone-yeast-extract (PYE) medium (39) for routine culturing. To control phosphate levels, *C. crescentus* was grown in Hutner-Imidazole-Glucose-Glutamate (HIGG) media with variable amounts of phosphate (1-1000 μM) (40). *E. coli* strains were grown at 37 °C in LB medium.

When necessary, antibiotics were added at the following concentrations: kanamycin 30 µg/ml in broth and 50 µg/ml in agar (abbreviated 30:50) for *E. coli* and 5:25 for *C. crescentus*; ampicillin 50:100 *E. coli*; tetracycline 12:12 *E. coli* and 1:2 *C. crescentus*; gentamicin 15:20 *E. coli* and 0.5:5 *C. crescentus*; spectinomycin 50:50 *E. coli* and 25:100 *C. crescentus*. Gene expression was induced in *C. crescentus* with either 0.3% (w/v) xylose or 0.5 mM vanillate. *E. coli* gene expression was induced with isopropyl β-D-1-thiogalactopyranoside (IPTG; 1mM). Phage titering was performed by adding 1-10 µl of ΦCr30 to 100 µl of an overnight culture of NA1000 in PYE. This mixture was added to 4 ml of soft agar (0.3% w/v agar in PYE) and overlaid on a PYE-agar plate. After solidifying, the plate was incubated overnight at 30 °C and plaques were counted.

Microscopy and image analysis

Cells were spotted onto 1% agarose pads made in the corresponding growth medium. Phase microscopy was performed on a Nikon TiE inverted microscope equipped with a Prior Lumen 220PRO illumination system, Zyla sCMOS 5.5-megapixel camera, CFI Plan Apochromat 100X oil immersion objective (NA 1.45, WD 0.13 mm), and NIS Elements software for image acquisition. Cell and stalk dimensions were measured using *Morphometrics* (41) and ImageJ v. 1.48q (NIH), respectively. To measure membrane permeability, cells were grown in the presence of 1 µg/ml propidium iodide. EPS production was assessed as previously described (29). Briefly, cells were grown in HIGG-1 µM phosphate, collected 500 µl by centrifugation (14,000 x *g*, 5 min), and resuspended in 30 µl 0.5X PBS. 10 µl of the cell suspension was mixed with 5 µl FITC-dextran (10 mg/ml, 2 MDa MW, Sigma) and 1 µl SlowFade Diamond mountant (Thermo

Scientific). 2 µl of this mixture was spotted onto a glass slide, cover-slipped, and sealed with VALAP (1:1:1 vaseline:lanolin:paraffin) for imaging.

Quantitative RT-PCR (qRT-PCR)

RNA was extracted from bacterial cultures using the Qiagen RNeasy kit. Following DNase digestion, RNA (5 ng/µl) was reverse transcribed using the High Capacity cDNA Reverse Transcription Kit (Applied Biosystems). 1 µl of cDNA was used as a template in a 10 µl qRT-PCR reaction performed with Power SYBR reagent (Applied Biosystems). qRT-PCR was performed on an ABI QuantStudio 6 using the ΔΔCt method. *rpoD* expression was used as the loading control.

Lipid extraction

C. crescentus strains were grown in 500 ml of HIGG with either 1 mM or 1 µM phosphate until reaching stationary phase. Sgt1/2 *E. coli* expression strains were grown overnight in 500 ml LB media with 1 mM IPTG to induce protein expression. Lipids were extracted by the method of Bligh and Dyer (42). Cells were harvested in glass tubes at 10,000 x *g* for 30 min and the majority of the supernatant was removed; stalked *C. crescentus* are very buoyant and do not form tight pellets preventing the complete removal of supernatant. The cells were resuspended in the residual supernatant, 3.75 volumes of 1:2 (v/v) chloroform: methanol was added, and the samples were mixed by vortexing. Chloroform (1.25 volumes) and water (1.25 volumes) were added sequentially with vortexing to create a two-phase system and the samples were centrifuged at 200 x *g* for 5 minutes at room temperature. The bottom, organic phase was transferred to a

clean tube with a Pasteur pipette and washed twice in "authentic" upper-phase. Subsequently, the residual organic phase with the lipids was collected and dried under argon.

Liquid chromatography/tandem mass spectrometry (LC/ESI–MS/MS)

Methods for LC/ESI–MS/MS have been described (43, 44). Briefly, normal phase LC was performed on an Agilent 1200 Quaternary LC system equipped with an Ascentis Silica HPLC column, 5 µm, 25 cm × 2.1 mm (Sigma-Aldrich, St. Louis, MO) as described. The LC eluent (with a total flow rate of 300 µl/min) was introduced into the ESI source of a high resolution TripleTOF5600 mass spectrometer (Applied Biosystems, Foster City, CA). Instrumental settings for negative ion ESI and MS/MS analysis of lipid species were as follows: IS = −4500 V; CUR = 20 psi; GSI = 20 psi; DP = −55 V; and FP = −150 V. The MS/MS analysis used nitrogen as the collision gas. Data analysis was performed using Analyst TF1.5 software (Applied Biosystems, Foster City, CA).

Growth curve analysis

For polymyxin B sensitivity assays, *C. crescentus* cells were diluted to OD_{660} = 0.05 in HIGG- 1 mM or 1 µM phosphate, treated with 30 µg/ml polymyxin B, and incubated with shaking (250 rpm, 30 °C). Complementation gene expression was induced with 0.3% xylose. Samples were taken at the indicated times for absorbance measurements (OD_{660}). For phage sensitivity assays, cells were grown in PYE and diluted to OD_{660} = 0.05. 148 µl of culture was dispensed per well in a 96-well plate. To each well, 2 µl of water (control) or ΦCr30 ($5x10^5$ pfu/ml final concentration) was added. To prevent evaporation, each well was overlaid with 100 µl mineral

oil. OD_{660} was recorded every 20 minutes on a BMG Labtech CLARIOstar plate reader incubating at 30 °C with continuous shaking.

Phage adsorption and burst-size quantification

Phage adsorption and burst-size were measured essentially as previously described (25). To measure phage adsorption, cells were grown in HIGG- 1 μM phosphate and diluted to OD_{660} = 0.2. Cells (1 ml) were aliquoted into glass culture tubes and 10^5 pfu ΦCr30 was added. Cultures were incubated with shaking at 30 °C; at various time points, 10 μl of culture was removed and diluted into 1 ml water: chloroform 9:1 (v/v). 10 μl of this mixture was used to titer the unbound phage as described above. To measure viral burst size, cells were grown in HIGG- 1 μM phosphate and diluted to OD_{660} = 0.1. Cells (0.5 ml) were infected with 0.5 x 10^5 pfu ΦCr30 and incubated at 30 °C for 15 min. The culture was diluted 1000-fold into HIGG- 1 μM phosphate; a 200 μl aliquot was removed every 15 min for titering as described above.

SDS-PAGE and protein staining

E. coli strains were grown overnight in LB media with 1 mM IPTG to induce protein expression. 500 μl of each strain was collected by centrifugation (6,000 x *g* for 2 min) and resuspended in 100 μl sample buffer. Protein samples were resolved on a 12% SDS-PAGE gel and stained with Coomassie blue for visualization.

Lipopolysaccharide (LPS) purification and analysis

LPS was purified essentially as previously described (45). Briefly, 5 ml of *C. crescentus* cells grown in HIGG- 1 μM phosphate (OD_{660} = 0.5) were collected and washed once in 10 mM

HEPES, pH 7.2. Cells were resuspended in 250 µl TE buffer (10 mM Tris, 1 mM EDTA, pH 7.2) and frozen overnight at -20 °C. Cells were thawed, treated with 1 µl DNase (0.5 mg/ml), 20 µl lysozyme (10 mg/ml), and 3 µl $MgCl_2$ (1M), and incubated at room temperature for 15 minutes. For each sample, 36.25 µl was mixed with 12.5 µl 4X SDS-sample buffer and boiled at 100 °C for 10 minutes. After cooling to room temperature, 1.25 µl proteinase K (20 mg/ml) was added and samples were incubated at 60 °C for 1 hour. LPS samples were resolved on a 12% SDS-PAGE gel and stained with the Pro-Q Emerald 300 LPS stain kit according to the manufacturer's protocol (Thermo Scientific). Images were acquired on a Bio-Rad ChemiDoc MP using UV excitation and a 530 nm emission filter.

S-Layer (RsaA) purification and analysis

RsaA was purified essentially as previously described (46). Briefly, cells were grown overnight in HIGG- 1 µM phosphate and 5 ml (OD_{660} = 0.6) were collected by centrifugation. The cell pellets were washed twice in 5 ml of 10 mM HEPES (pH 7.2), resuspended in 200 µl 100 mM HEPES (pH 2), and incubated at room temperature for 10 minutes. Cells were pelleted (10 min, 5,000 x *g*) and the supernatant containing RsaA was collected and neutralized with 2.8 µl 10N NaOH. RsaA samples in 1X sample buffer were resolved on a 7.5% SDS-PAGE gel without heat-denaturing and stained with Krypton protein stain (Thermo Scientific). Images were acquired on a Bio-Rad ChemiDoc MP using green LED excitation and a 605 nm emission filter.

Acknowledgements

We thank Yves Brun (Indiana University) for providing strains. Funding was provided by National Science Foundation CAREER Award MCB-1553004 (to E.A.K.) and National Institutes of Health grants GM069338 and EY023666 (to Z.G.).

References

1. Marr AG, Ingraham JL. 1962. Effect of temperature on the composition of fatty acids in *Escherichia coli*. J Bacteriol 84:1260-7.
2. Sinensky M. 1974. Homeoviscous adaptation--a homeostatic process that regulates the viscosity of membrane lipids in *Escherichia coli*. Proc Natl Acad Sci U S A 71:522-5.
3. Romantsov T, Guan Z, Wood JM. 2009. Cardiolipin and the osmotic stress responses of bacteria. Biochim Biophys Acta 1788:2092-100.
4. Tsatskis Y, Khambati J, Dobson M, Bogdanov M, Dowhan W, Wood JM. 2005. The osmotic activation of transporter ProP is tuned by both its C-terminal coiled-coil and osmotically induced changes in phospholipid composition. J Biol Chem 280:41387-94.
5. Carlsson P, Caron DA. 2001. Seasonal variation of phosphorus limitation of bacterial growth in a small lake. Limnology and Oceanography 46:108-120.
6. Schlimpert S, Klein EA, Briegel A, Hughes V, Kahnt J, Bolte K, Maier UG, Brun YV, Jensen GJ, Gitai Z, Thanbichler M. 2012. General protein diffusion barriers create compartments within bacterial cells. Cell 151:1270-82.
7. Klein EA, Schlimpert S, Hughes V, Brun YV, Thanbichler M, Gitai Z. 2013. Physiological role of stalk lengthening in *Caulobacter crescentus*. Commun Integr Biol 6:e24561.

8. Wagner JK, Setayeshgar S, Sharon LA, Reilly JP, Brun YV. 2006. A nutrient uptake role for bacterial cell envelope extensions. Proc Natl Acad Sci U S A 103:11772-7.

9. De Siervo AJ, Homola AD. 1980. Analysis of *Caulobacter crescentus* lipids. J Bacteriol 143:1215-22.

10. Geske T, Vom Dorp K, Dormann P, Holzl G. 2013. Accumulation of glycolipids and other non-phosphorous lipids in *Agrobacterium tumefaciens* grown under phosphate deprivation. Glycobiology 23:69-80.

11. Semeniuk A, Sohlenkamp C, Duda K, Holzl G. 2014. A bifunctional glycosyltransferase from *Agrobacterium tumefaciens* synthesizes monoglucosyl and glucuronosyl diacylglycerol under phosphate deprivation. J Biol Chem 289:10104-14.

12. Devers EA, Wewer V, Dombrink I, Dormann P, Holzl G. 2011. A processive glycosyltransferase involved in glycolipid synthesis during phosphate deprivation in *Mesorhizobium loti*. J Bacteriol 193:1377-84.

13. Kato M, Muto Y, Tanaka-Bandoh K, Watanabe K, Ueno K. 1995. Sphingolipid Composition in Bacteroides Species. Anaerobe 1:135-139.

14. Kawahara K, Moll H, Knirel YA, Seydel U, Zähringer U. 2000. Structural analysis of two glycosphingolipids from the lipopolysaccharide-lacking bacterium *Sphingomonas capsulata*. European Journal of Biochemistry 267:1837-1846.

15. Kawahara K, Lindner B, Isshiki Y, Jakob K, Knirel YA, Zähringer U. 2001. Structural analysis of a new glycosphingolipid from the lipopolysaccharide-lacking bacterium *Sphingomonas adhaesiva*. Carbohydrate Research 333:87-93.

16. Hanada K. 2003. Serine palmitoyltransferase, a key enzyme of sphingolipid metabolism. Biochim Biophys Acta 1632:16-30.

435 17. Kihara A, Mitsutake S, Mizutani Y, Igarashi Y. 2007. Metabolism and biological
436 functions of two phosphorylated sphingolipids, sphingosine 1-phosphate and ceramide 1-
437 phosphate. Prog Lipid Res 46:126-44.
438 18. Geiger O, Gonzalez-Silva N, Lopez-Lara IM, Sohlenkamp C. 2010. Amino acid-
439 containing membrane lipids in bacteria. Prog Lipid Res 49:46-60.
440 19. Christen B, Abeliuk E, Collier JM, Kalogeraki VS, Passarelli B, Coller JA, Fero MJ,
441 McAdams HH, Shapiro L. 2011. The essential genome of a bacterium. Mol Syst Biol 7:1-
442 7.
443 20. Ikushiro H, Nagami A, Takai T, Sawai T, Shimeno Y, Hori H, Miyahara I, Kamiya N,
444 Yano T. 2018. Heme-dependent Inactivation of 5-Aminolevulinate Synthase from
445 *Caulobacter crescentus*. Sci Rep 8:14228.
446 21. Lombard V, Golaconda Ramulu H, Drula E, Coutinho PM, Henrissat B. 2013. The
447 carbohydrate-active enzymes database (CAZy) in 2013. Nucleic Acids Res 42:D490-5.
448 22. Lubin EA, Henry JT, Fiebig A, Crosson S, Laub MT. 2016. Identification of the PhoB
449 regulon and role of PhoU in the phosphate starvation response of *Caulobacter crescentus*.
450 J Bacteriol 198:187-200.
451 23. Li C, Tan BK, Zhao J, Guan Z. 2016. In vivo and in vitro synthesis of
452 phosphatidylglycerol by an *Escherichia coli* cardiolipin synthase. J Biol Chem
453 291:25144-25153.
454 24. Vaz-Moreira I, Nunes OC, Manaia CM. 2011. Diversity and antibiotic resistance patterns
455 of Sphingomonadaceae isolates from drinking water. Appl Environ Microbiol 77:5697-
456 706.

457 25. Ely B, Johnson RC. 1977. Generalized transduction in *Caulobacter crescentus*. Genetics
458 87:391-9.
459 26. Smith MCM, Rees CED, Sockett RE. 1999. Exploitation of bacteriophages and their
460 components, p 97-132, Methods in Microbiology, vol 29. Academic Press.
461 27. Edwards P, Smit J. 1991. A transducing bacteriophage for *Caulobacter crescentus* uses
462 the paracrystalline surface layer protein as a receptor. J Bacteriol 173:5568-72.
463 28. Walker SG, Karunaratne DN, Ravenscroft N, Smit J. 1994. Characterization of mutants
464 of *Caulobacter crescentus* defective in surface attachment of the paracrystalline surface
465 layer. J Bacteriol 176:6312-23.
466 29. Herr KL, Carey AM, Heckman TI, Chavez JL, Johnson CN, Harvey E, Gamroth WA,
467 Wulfing BS, Van Kessel RA, Marks ME. 2018. Exopolysaccharide production in
468 *Caulobacter crescentus*: A resource allocation trade-off between protection and
469 proliferation. PLoS One 13:e0190371.
470 30. Gonin M, Quardokus EM, O'Donnol D, Maddock J, Brun YV. 2000. Regulation of stalk
471 elongation by phosphate in *Caulobacter crescentus*. J Bacteriol 182:337-347.
472 31. Kawahara K, Kubota M, Sato N, Tsuge K, Seto Y. 2002. Occurrence of an alpha-
473 galacturonosyl-ceramide in the dioxin-degrading bacterium *Sphingomonas wittichii*.
474 FEMS Microbiol Lett 214:289-294.
475 32. Luo H, Lin Y, Gao F, Zhang CT, Zhang R. 2014. DEG 10, an update of the database of
476 essential genes that includes both protein-coding genes and noncoding genomic elements.
477 Nucleic Acids Res 42:D574-80.
478 33. Altschul SF, Gish W, Miller W, Myers EW, Lipman DJ. 1990. Basic local alignment
479 search tool. J Mol Biol 215:403-10.

480 34. Holzl G, Leipelt M, Ott C, Zahringer U, Lindner B, Warnecke D, Heinz E. 2005.
481 Processive lipid galactosyl/glucosyltransferases from *Agrobacterium tumefaciens* and
482 *Mesorhizobium loti* display multiple specificities. Glycobiology 15:874-86.
483 35. Jorasch P, Warnecke DC, Lindner B, Zahringer U, Heinz E. 2000. Novel processive and
484 nonprocessive glycosyltransferases from *Staphylococcus aureus* and *Arabidopsis*
485 *thaliana* synthesize glycoglycerolipids, glycophospholipids, glycosphingolipids and
486 glycosylsterols. Eur J Biochem 267:3770-83.
487 36. Yan A, Guan Z, Raetz CR. 2007. An undecaprenyl phosphate-aminoarabinose flippase
488 required for polymyxin resistance in *Escherichia coli*. J Biol Chem 282:36077-89.
489 37. Herrmann J, Jabbarpour F, Bargar PG, Nomellini JF, Li PN, Lane TJ, Weiss TM, Smit J,
490 Shapiro L, Wakatsuki S. 2017. Environmental calcium controls alternate physical states
491 of the *Caulobacter* surface layer. Biophys J 112:1841-1851.
492 38. Amat F, Comolli LR, Nomellini JF, Moussavi F, Downing KH, Smit J, Horowitz M.
493 2010. Analysis of the intact surface layer of *Caulobacter crescentus* by cryo-electron
494 tomography. J Bacteriol 192:5855-65.
495 39. Poindexter JS. 1964. Biological properties and classification of the *Caulobacter* group.
496 Bacteriol Rev 28:231-95.
497 40. Poindexter JS. 1978. Selection for nonbuoyant morphological mutants of *Caulobacter*
498 *crescentus*. J Bacteriol 135:1141-5.
499 41. Ursell T, Lee TK, Shiomi D, Shi H, Tropini C, Monds RD, Colavin A, Billings G,
500 Bhaya-Grossman I, Broxton M, Huang BE, Niki H, Huang KC. 2017. Rapid, precise
501 quantification of bacterial cellular dimensions across a genomic-scale knockout library.
502 BMC Biol 15:17.

503 42. Bligh EG, Dyer WJ. 1959. A rapid method of total lipid extraction and purification. Can J
504 Biochem Physiol 37:911-7.
505 43. Goldfine H, Guan Z. 2015. Lipidomic Analysis of Bacteria by Thin-Layer
506 Chromatography and Liquid Chromatography/Mass Spectrometry, p 1-15. *In* McGenity
507 TJ (ed), Hydrocarbon and Lipid Microbiology Protocols doi:10.1007/8623_2015_56.
508 Humana Press.
509 44. Guan Z, Katzianer D, Zhu J, Goldfine H. 2014. *Clostridium difficile* contains
510 plasmalogen species of phospholipids and glycolipids. Biochim Biophys Acta
511 1842:1353-9.
512 45. Cabeen MT, Murolo MA, Briegel A, Bui NK, Vollmer W, Ausmees N, Jensen GJ,
513 Jacobs-Wagner C. 2010. Mutations in the Lipopolysaccharide biosynthesis pathway
514 interfere with crescentin-mediated cell curvature in *Caulobacter crescentus*. J Bacteriol
515 192:3368-78.
516 46. Walker SG, Smith SH, Smit J. 1992. Isolation and comparison of the paracrystalline
517 surface layer proteins of freshwater *Caulobacters*. J Bacteriol 174:1783-92.

518

519

Figure Legends

Figure 1: Phosphate starvation alters *C. crescentus* lipid composition. (A) Phase-contrast images of *C. crescentus* grown in HIGG media with either 1 mM or 1 μM phosphate. Scale bar: 2 μm. (B) Total ion chromatograms of lipids from *C. crescentus* grown in HIGG media with either 1 mM or 1 μM phosphate. Phosphate starvation induces the production of a HexHexA-ceramide lipid. (C) Structures of bacterial glycosphingolipids. GSL-1,-3, and -4 are found in *Sphingomonas* species (14, 15). GSL-2 is a novel *C. crescentus* glycosphingolipid. The structural drawing of GSL-2 is for illustration purposes; the orientations of the hydroxyl groups have not been determined. GlcA- glucuronic acid; Gal- galactose; GlcN- glucosamine; Man- mannose; R-ceramide lipid.

Figure 2: CCNA_01220 is required for ceramide synthesis. Wild-type, Δ*ccna_01220*, and *Δccna_01647* cells were grown in HIGG- 1μM phosphate and total lipids were isolated. Negative ion ESI/MS shows the $[M + Cl]^-$ ions of the lipids (ceramide and MHDAG) emerging at 2.4 to 4.0 min.

Figure 3: Identification of sphingolipid glycosyltransferases. (A) qRT-PCR of candidate glycosyltransferases *ccna_00792* and *ccna_00793* was performed on samples from *C. crescentus* grown in HIGG-1 mM or 1 μM phosphate. The graph represents the fold induction seen in 1 μM phosphate relative to 1 mM phosphate. mRNA levels are normalized to *rpoD* expression. Error bars are the standard error, n=3. (B) RNA was extracted from wild-type and Δ*phoB* cells grown in HIGG-1 μM phosphate and analyzed by qRT-PCR. mRNA levels are normalized to *rpoD*

543 expression. Error bars are the standard error, n=3. *p=0.04, **p<10^{-5}; two-tailed *t*-test. (C-D)
544 Wild-type, Δ*ccna_00792*, and *Δccna_00793* cells were grown in HIGG- 1μM phosphate and
545 total lipids were isolated. Negative ion ESI/MS shows the $[M-H]^-$ and $[M + Cl]^-$ ions of the
546 lipids emerging at 18 to 20 min (C) and 14 to 17 min (D). (E) The LC/MS data support a model
547 of successive glycosylation of ceramide to HexA-Cer and HexHexA-Cer by Sgt1 and Sgt2,
548 respectively. The structural drawings are for illustration purposes; the orientations of the
549 hydroxyl groups have not been determined.
550
551 **Figure 4: Ectoptic production of glycosphingolipids is detrimental to cell integrity.** (A-C)
552 Lipids were analyzed from strain GS81 (Sgt1/Sgt2 overexpression) grown in HIGG-1 mM
553 phosphate and induced with 0.3% xylose and 0.5 mM vanillate. (A) The total ion chromatogram
554 shows the simultaneous production of phospholipids and glycosphingolipids. Negative ion
555 ESI/MS showing the $[M-H]^-$ and $[M + Cl]^-$ ions of the lipids emerging at 14 to 15 min (B) and
556 17 to 19 min (C) confirms the synthesis of HexA-Cer and GSL-2. We note the presence of an
557 unknown lipid species with *m/z*=804.531. (D) Wild-type and Sgt1/2 overexpression cells were
558 grown in HIGG-1 mM phosphate and induced with 0.3% xylose and 0.5 mM vanillate. Cells
559 were labeled with 1 μg/ml propidium iodide and imaged by fluorescence microscopy. The
560 micrographs are overlays of phase and fluorescence images. Scale bar: 10 μm.
561
562 **Figure 5: Ceramides regulate polymyxin B resistance and phage susceptibility. (**A-B)
563 Growth curves for the indicated strains were measured in HIGG- 1 mM phosphate (A) or 1 μM
564 phosphate (B). Cells were grown in the presence of polymyxin B (PMX; 10 μg/ml) or water
565 (control). Complementation strains were induced with 0.3% xylose. Error bars are the standard

566 error, n=3. (C) Growth curves for wild-type and Δ*ccbF* cells were measured in PYE in the
567 presence of phage ΦCr30 ($5x10^5$ pfu/ml) or water (control). Error bars are the standard error,
568 n=3. (D) Phage adsorption was measured for the indicated strains in HIGG- 1 μM phosphate.
569 Complementation strains were induced with 0.3% xylose. Error bars are the standard error, n≥4.
570 (E) Phage burst-size was measured for the indicated strains in HIGG- 1 μM phosphate. Phage
571 titer was recorded over time (left panel) and the fold-increase from the initial titer was calculated
572 as the burst size (right panel). Error bars are the standard error, n=3.
573

Supplemental materials

Supplemental text:

- Detailed description of strain construction
- Supplemental references

Table S1: List of strains used in this manuscript

Table S2: List of plasmids used in this manuscript

Table S3: List of primers used in this manuscript

Table S4: Selection criteria for assessing candidate glycosyltransferases

Figure S1: LC/MS confirmation of gene complementation

Figure S2: Expression of Sgt1/2 in *E. coli*

Figure S3: Ceramides are not required for stalk or cell body elongation

Figure S4: Depletion of GSLs does not affect LPS, S-layer, or EPS production

Figure 1

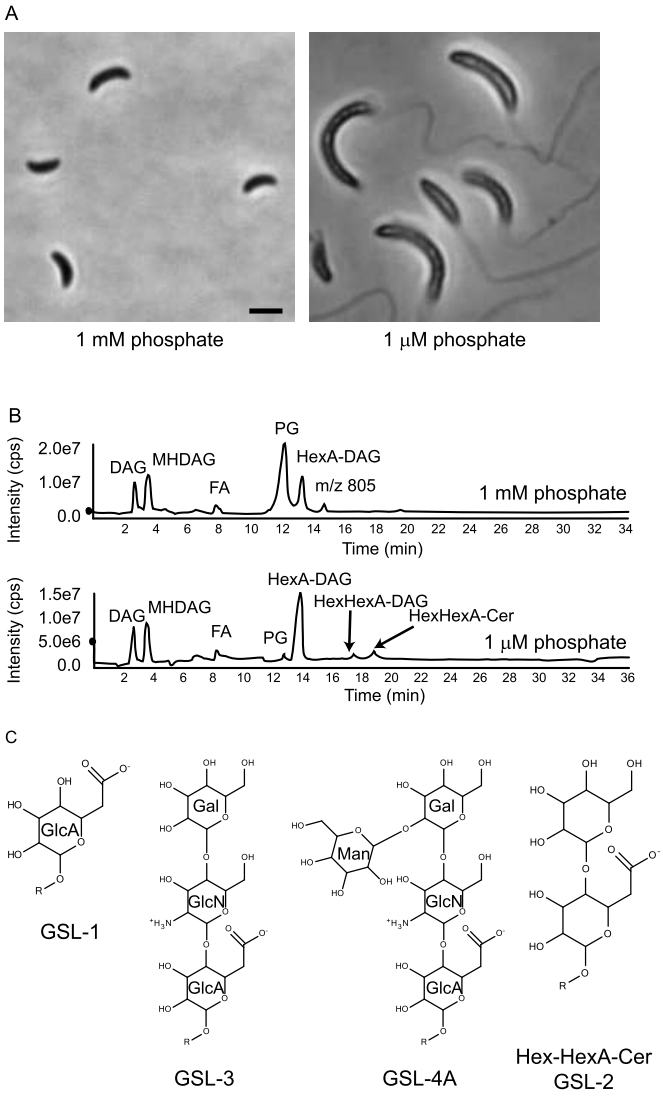
A
1 mM phosphate
1 μM phosphate
B
Intensity (cps)
2.0e7
1.0e7
0.0
DAG
MHDAG
FA
PG
HexA-DAG
m/z 805
1 mM phosphate
Time (min)
1.5e7
1.0e7
5.0e6
0.0
HexA-DAG
HexHexA-DAG
HexHexA-Cer
1 μM phosphate
C
GSL-1
GSL-3
GSL-4A
Hex-HexA-Cer
GSL-2
GlcA
Gal
GlcN
Man

Figure 2

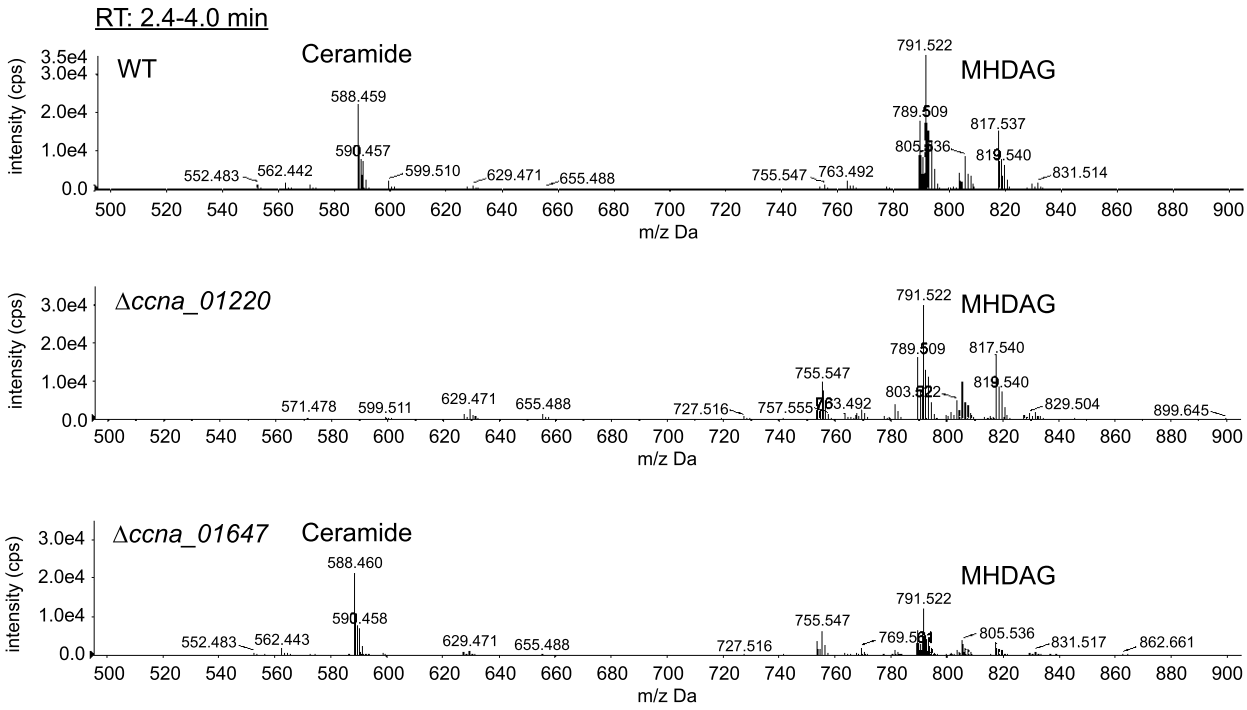
RT: 2.4-4.0 min
WT
Ceramide
MHDAG
intensity (cps)
m/z Da
588.459
590.457
791.522
789.509
817.537
805.536
819.540
552.483
562.442
599.510
629.471
655.488
755.547
763.492
831.514
Δccna_01220
571.478
727.516
803.522
829.504
899.645
Δccna_01647
588.460
590.458
562.443
769.501
862.661

Figure 3

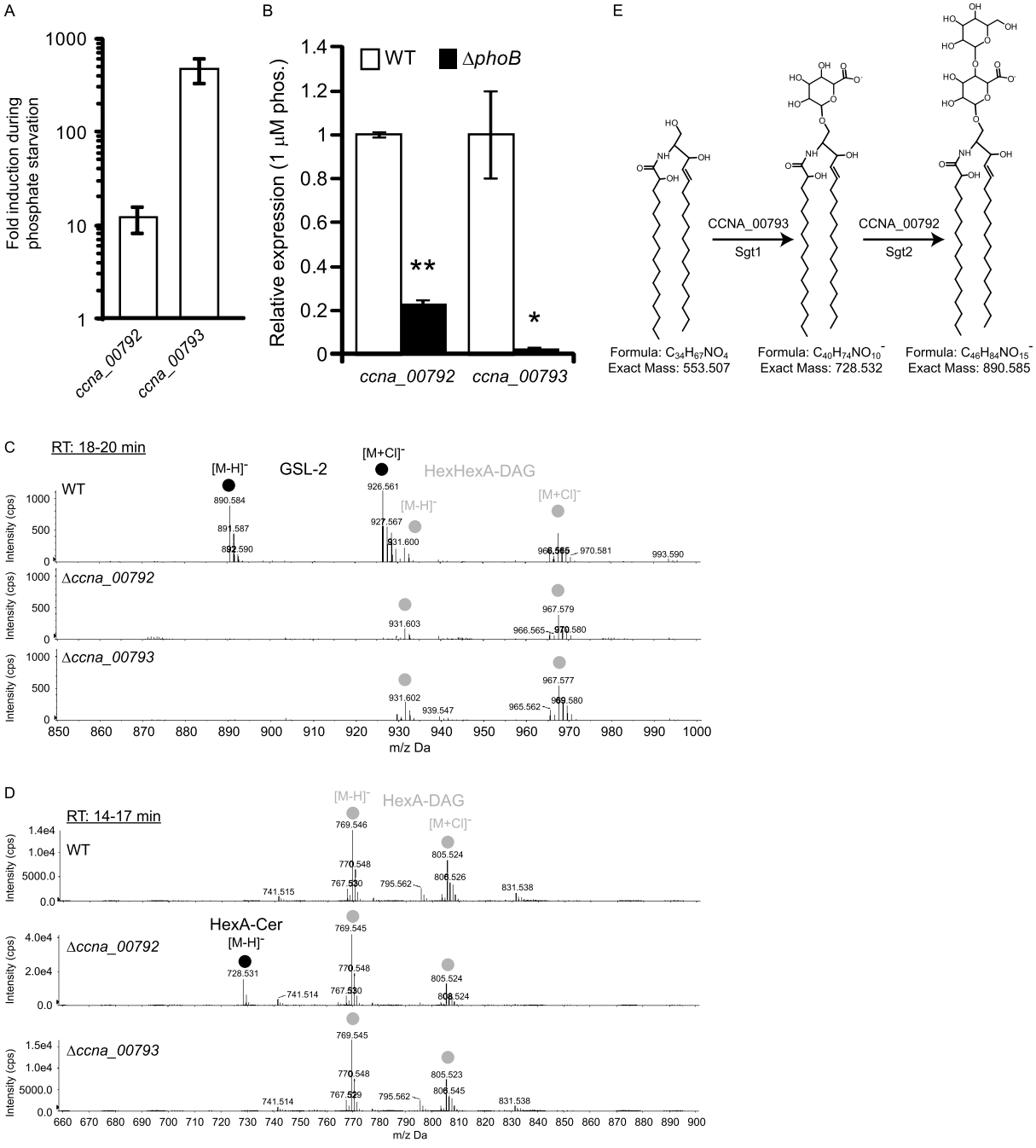
A
Fold induction during phosphate starvation
1000
100
10
1
ccna_00792
ccna_00793
B
Relative expression (1 µM phos.)
WT
ΔphoB
1.4
1.2
1
0.8
0.6
0.4
0.2
0
**
*
ccna_00792
ccna_00793
E
CCNA_00793
Sgt1
CCNA_00792
Sgt2
Formula: C34H67NO4
Exact Mass: 553.507
Formula: C40H74NO10-
Exact Mass: 728.532
Formula: C46H84NO15-
Exact Mass: 890.585
C
RT: 18-20 min
GSL-2
HexHexA-DAG
[M-H]-
[M+Cl]-
WT
Δccna_00792
Δccna_00793
Intensity (cps)
m/z Da
D
RT: 14-17 min
HexA-DAG
HexA-Cer
WT
Δccna_00792
Δccna_00793
Intensity (cps)
m/z Da

Figure 4

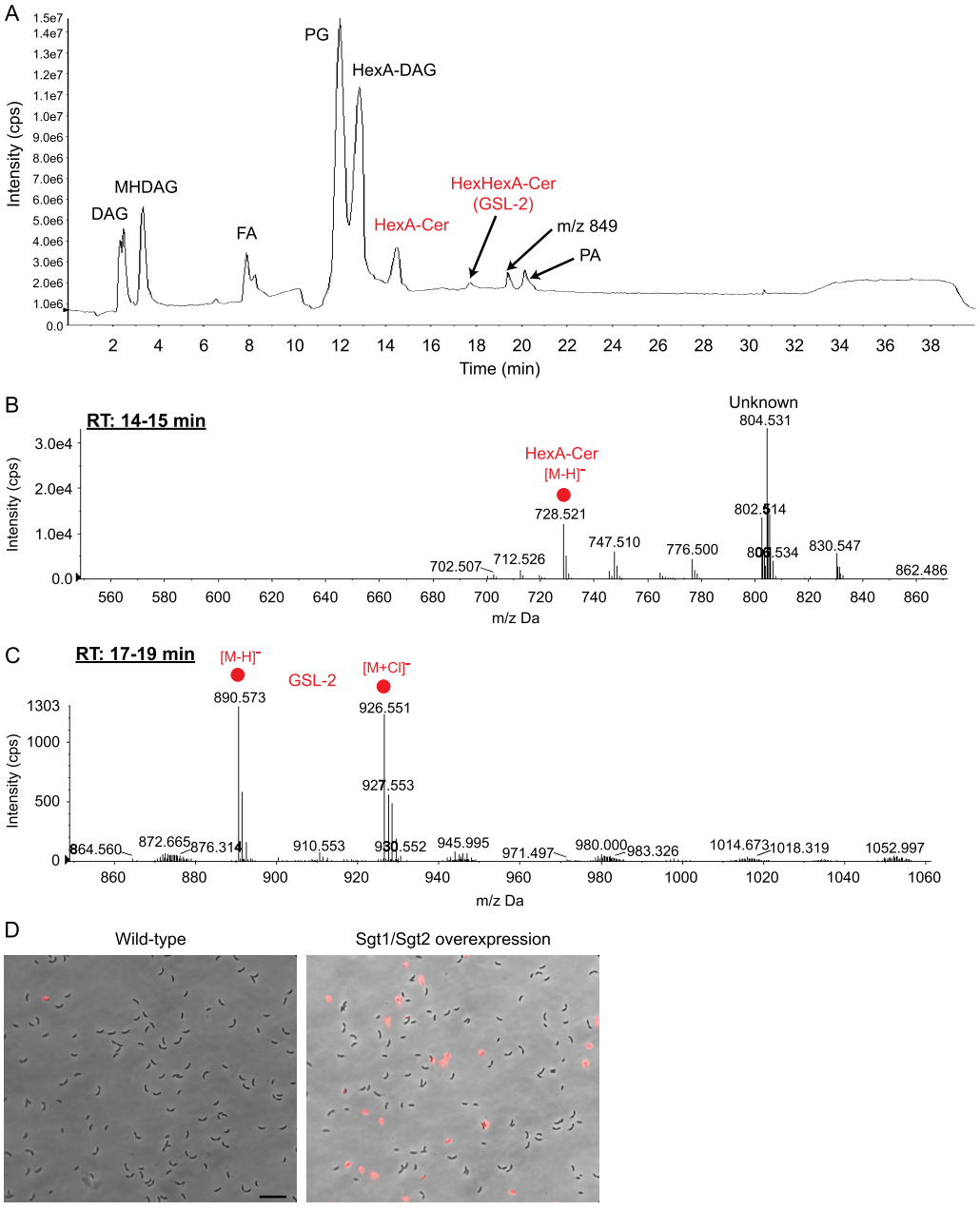
A
Intensity (cps)
Time (min)
PG
HexA-DAG
MHDAG
DAG
FA
HexA-Cer
HexHexA-Cer
(GSL-2)
m/z 849
PA
B
RT: 14-15 min
Intensity (cps)
m/z Da
Unknown
804.531
HexA-Cer
[M-H]⁻
728.521
802.514
747.510
776.500
830.547
702.507
712.526
862.486
C
RT: 17-19 min
[M-H]⁻
GSL-2
[M+Cl]⁻
890.573
926.551
927.553
Intensity (cps)
m/z Da
864.560
872.665
876.314
910.553
945.995
971.497
980.000
983.326
1014.673
1018.319
1052.997
D
Wild-type
Sgt1/Sgt2 overexpression

Figure 5

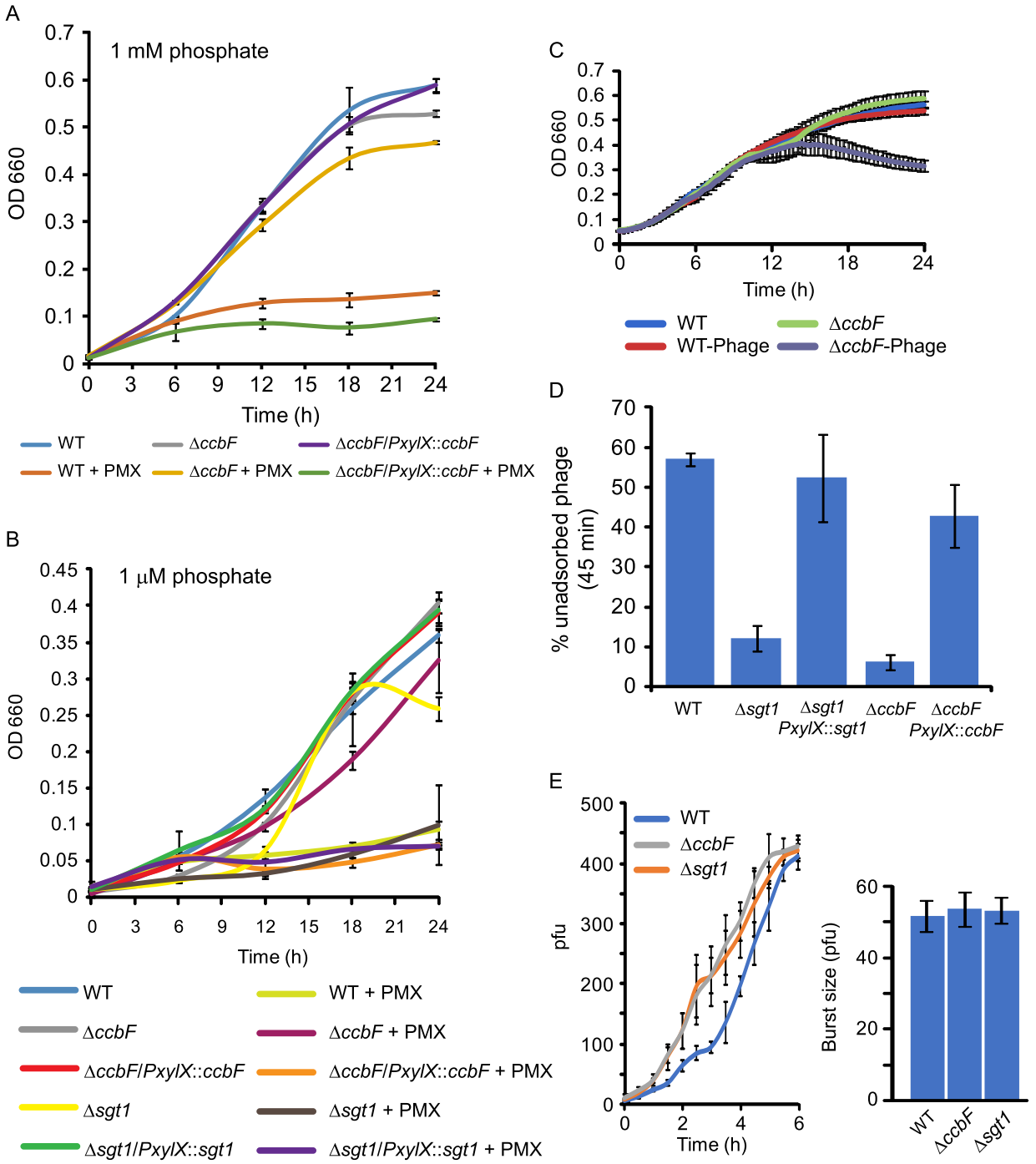
A
1 mM phosphate
OD 660
Time (h)
WT
ΔccbF
ΔccbF/PxylX::ccbF
WT + PMX
ΔccbF + PMX
ΔccbF/PxylX::ccbF + PMX
B
1 μM phosphate
OD 660
Time (h)
WT
ΔccbF
ΔccbF/PxylX::ccbF
Δsgt1
Δsgt1/PxylX::sgt1
WT + PMX
ΔccbF + PMX
ΔccbF/PxylX::ccbF + PMX
Δsgt1 + PMX
Δsgt1/PxylX::sgt1 + PMX
C
OD 660
Time (h)
WT
WT-Phage
ΔccbF
ΔccbF-Phage
D
% unadsorbed phage (45 min)
WT
Δsgt1
Δsgt1 PxylX::sgt1
ΔccbF
ΔccbF PxylX::ccbF
E
pfu
Time (h)
WT
ΔccbF
Δsgt1
Burst size (pfu)
WT
ΔccbF
Δsgt1